HAL
archives-ouvertes.fr

Inverse Problem Approach for the Alignment of Electron Tomographic Series.

Viet Dung Tran, Maxime Moreaud, Éric Thiébaut, L. Denis, Jean-Marie Becker

▶ **To cite this version:**

Viet Dung Tran, Maxime Moreaud, Éric Thiébaut, L. Denis, Jean-Marie Becker. Inverse Problem Approach for the Alignment of Electron Tomographic Series.. Oil & Gas Science and Technology - Revue d'IFP Energies nouvelles, Institut Français du Pétrole, 2014, 69 (2), pp. 279-291. <10.2516/ogst/2013116>. <hal-00992251>

HAL Id: hal-00992251
https://hal-ifp.archives-ouvertes.fr/hal-00992251

Submitted on 16 May 2014

HAL is a multi-disciplinary open access archive for the deposit and dissemination of scientific research documents, whether they are published or not. The documents may come from teaching and research institutions in France or abroad, or from public or private research centers.

L'archive ouverte pluridisciplinaire **HAL**, est destinée au dépôt et à la diffusion de documents scientifiques de niveau recherche, publiés ou non, émanant des établissements d'enseignement et de recherche français ou étrangers, des laboratoires publics ou privés.

Oil & Gas Science and Technology – Rev. IFP Energies nouvelles, Vol. 69 (2014), No. 2, pp. 279-291
Copyright © 2013, IFP Energies nouvelles
DOI: 10.2516/ogst/2013116

Dossier

Advances in Signal Processing and Image Analysis for Physico-Chemical, Analytical Chemistry and Chemical Sensing
Progrès en traitement des signaux et analyse des images pour les analyses physico-chimiques et la détection chimique

Inverse Problem Approach for the Alignment of Electron Tomographic Series

V.-D. Tran[1,2*], M. Moreaud[1], É. Thiébaut[3], L. Denis[2] and J.M. Becker[2]

[1] *IFP Energies nouvelles, Rond-point de l'échangeur de Solaize, BP 3, 69360 Solaize - France*
[2] *Laboratoire Hubert Curien, UMR CNRS 5516, Université de Saint-Étienne - France*
[3] *Observatoire de Lyon, CRAL CNRS UMR 5574, Université de Lyon - France*
e-mail: viet-dung.tran@ifpen.fr - maxime.moreaud@ifpen.fr - eric.thiebaut@univ-lyon1.fr - loic.denis@univ-st-etienne.fr - becker@cpe.fr

* Corresponding author

Résumé — **Approche problème inverse pour l'alignement de séries en tomographie électronique** — Dans le domaine du raffinage, les mesures morphologiques de particules sont devenues indispensables pour caractériser les supports de catalyseurs. À travers ces paramètres, on peut remonter aux spécificités physico-chimiques des matériaux étudiés. Une des techniques d'acquisition utilisées est la tomographie électronique (ou nanotomographie). Des volumes 3D sont reconstruits à partir de séries de projections sous différents angles obtenues par Microscopie Électronique en Transmission (MET). Cette technique permet d'obtenir une réelle information tridimensionnelle à l'échelle du nanomètre. Un problème majeur dans ce contexte est le mauvais alignement des projections qui contribuent à la reconstruction. Les techniques d'alignement actuelles emploient habituellement des marqueurs de réference tels que des nanoparticules d'or pour un alignement correct des images. Lorsque l'utilisation de marqueurs n'est pas possible, l'alignement de projections adjacentes est obtenu par corrélation entre ces projections. Cependant, cette méthode échoue parfois. Dans cet article, nous proposons une nouvelle méthode basée sur une approche de type problème inverse où un certain critère est minimisé en utilisant une variante de l'algorithme de Nelder et Mead, qui exploite le concept de simplexe. Elle est composée de deux étapes. La première étape consiste en un processus d'alignement initial s'appuyant sur la minimisation d'une fonction de coût basée sur des statistiques robustes, mesurant la similarité entre une projection et les projections précédentes de la série. Elle vise à réduire les forts déplacements, résultant de l'acquisition entre les projections successives. Dans la seconde étape, les projections pré-recalées sont employées pour initialiser un processus itératif et alterné d'alignement et reconstruction, minimisant alternativement une fonction de coût basée sur la reconstruction du volume et une fonction basée sur l'alignement d'une projection avec sa version simulée obtenue à partir du volume reconstruit. À la fin de ce processus, nous obtenons une reconstruction correcte du volume, les projections étant correctement alignées. Notre méthode a été testée sur des données simulées et prouve qu'elle récupère d'une manière précise les changements dans les paramètres de translation, rotation et mise à l'échelle. Nous avons testé avec succès notre méthode pour les projections réelles de différents supports de catalyseur.

Abstract — ***Inverse Problem Approach for the Alignment of Electron Tomographic Series*** — *In the refining industry, morphological measurements of particles have become an essential part in the*

characterization catalyst supports. Through these parameters, one can infer the specific physicochemical properties of the studied materials. One of the main acquisition techniques is electron tomography (or nanotomography). 3D volumes are reconstructed from sets of projections from different angles made by a Transmission Electron Microscope (TEM). This technique provides a real three-dimensional information at the nanometric scale. A major issue in this method is the misalignment of the projections that contributes to the reconstruction. The current alignment techniques usually employ fiducial markers such as gold particles for a correct alignment of the images. When the use of markers is not possible, the correlation between adjacent projections is used to align them. However, this method sometimes fails. In this paper, we propose a new method based on the inverse problem approach where a certain criterion is minimized using a variant of the Nelder and Mead simplex algorithm. The proposed approach is composed of two steps. The first step consists of an initial alignment process, which relies on the minimization of a cost function based on robust statistics measuring the similarity of a projection to its previous projections in the series. It reduces strong shifts resulting from the acquisition between successive projections. In the second step, the pre-registered projections are used to initialize an iterative alignment-refinement process which alternates between (i) volume reconstructions and (ii) registrations of measured projections onto simulated projections computed from the volume reconstructed in (i). At the end of this process, we have a correct reconstruction of the volume, the projections being correctly aligned. Our method is tested on simulated data and shown to estimate accurately the translation, rotation and scale of arbitrary transforms. We have successfully tested our method with real projections of different catalyst supports.

INTRODUCTION

The term "tomography" refers to all methods of exact reconstruction or – most often – approached reconstruction of the interior of an object from its projections; in other words methods for obtaining information on the composition of an object from the measurements taken outside the object.

Electron tomography (EM) [1] is a very powerful characterization technique for the reconstruction of the 3D nanoscale structure of objects from a series of two-dimensional projections. A series of 2D TEM projections is acquired by tilting the specimen at various angles (usually in the range $\pm$ 70°, one projection every degree) around an axis perpendicular to the electron beam (*Fig. 1*).

The geometry of acquisition is parallel (*i.e.* the electron beam which crosses the sample is rectilinear). In such parallel configurations, simplest reconstruction techniques recast the volume reconstruction into a series of independent 2D reconstructions, each corresponding to a slice perpendicular to the detector. Three main approaches have been developed in tomography: Filtered Back-Projections (FBP) [2], algebraic reconstruction methods [3-5] and algorithms based on Fourier transform [6, 7].

These reconstruction methods require a precise alignment of the different projections. Because of mechanical imprecision and magnetic lenses defocus, neighboring projections may differ by a shift, a slight tilt and a change in magnification [8]. Currently, the most common alignment technique uses markers' tracking [9-11]. This method uses gold nanoparticles spread onto the surface of the specimen prior to imaging; these particles can be localized very accurately, even at high tilt angles, thanks to their round shape and their sharp contrast. Alignment with markers has two advantages. First, since markers positions measured over the full range of tilt angles are fit to a single set of projection equations, the alignment of the series of projections is guaranteed to be globally consistent. Secondly, the method can be adapted to correct anisotropic and non-uniform changes of the specimen during the tilt series [8]. However, the fiducial markers method has several practical disadvantages. It can be difficult to obtain an appropriate distribution of markers on the specimen, *i.e.* a distribution as homogeneous as possible, a necessary condition for proper alignment. For high-resolution reconstruction (*e.g.* reconstructed volume with voxels $< 1\,nm^3$), the size of gold nanoparticles (approximately 5 nm in diameter) becomes considerable and troublesome by masking an important part into the body of the reconstruction. Another disadvantage of markers is the need to track their positions accurately, which can be a very costly step. Certain approaches [12-14] are based on points of interest automatically extracted from the images, these points are then used to find the alignment parameters.

We deal here with the case where no such markers are used for alignment. This case can be handled by cross-correlation methods [15-18]. The principle of these techniques is based on the alignment between two images. Precisely, the first image of a series of projections is chosen as the reference image, then each image is aligned with the previous image in the series, thereby

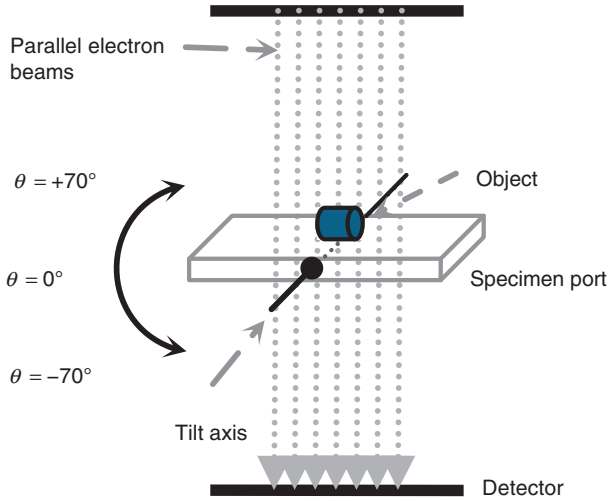

Figure 1

Data collection geometry in 3D reconstruction by TEM.

sequentially compensating image shifts throughout the entire series. Moreover, the accumulation of errors in the estimated parameters is a disadvantage of these methods based on pairwise alignment of images. To overcome this defect, a 3D model-based method is proposed by Dengler [19], in which the alignment parameters were refined by alternating a reconstruction step and an alignment step between the modeled projections and real projections. This method has been developed by several authors [20-22]. In cryoEM for the biological sciences, the 3D model-based method is known as a projection matching [23, 24], which also yields excellent results for X-ray tomography [25].

In this paper, we propose a new method for the alignment of TEM image series without the need for fiducial markers, which recovers in an accurate manner the changes in translation, rotation and scaling parameters. The alignment procedure consists of two stages:

– first, we use an optimization approach to align the series of projections. The aim is to reduce the strong shifts, resulting from the acquisition between successive projections, and to facilitate the following step;
– the pre-aligned projections are then used to initialize an iterative procedure which alternatively restores the 3-D object and accurately aligns the projections.

1 INITIAL ALIGNMENT

1.1 Alignment Between Two Images

Prior to the general case (global alignment of M images), one needs to build an alignment method for 2 images. Four transformation parameters are required: horizontal and vertical translations, rotation and scaling. These parameters define how an image I_t to be registered is transformed into a reference image I_r. We propose a method that is more robust than cross-correlation based approaches (see Appendix 2). This method finds the parameters of the geometrical transformations by minimizing the Mean Squared Error (MSE) between I_r and I_t:

$$\Delta\phi^* = \arg\min_{\Delta\phi} E(\Delta\phi) \tag{1}$$

with:

$$E(\Delta\phi) = \frac{1}{N}\sum_{i=1}^{N}\left[I_r(u_i) - (R_{\Delta\phi}\cdot I_t)(u_i)\right]^2 \tag{2}$$

The u_i are the pixels' coordinates, $R_{\Delta\phi}$ is a linear operator which interpolates its argument in order to apply a geometrical transformation of the image specified by the parameters $\Delta\phi = (\Delta u_x, \Delta u_y, \Delta\varphi, \Delta s)$ corresponding respectively to the horizontal and vertical shifts of a translation, the angle of a rotation and the magnification scale (*Sect. 1.2*). N is the number of pixels in the domain of interest (see *Fig. 2*), which depends on $\Delta\phi$. In our application, $\Delta u_x \in [-W/2, W/2]$ and $\Delta u_y \in [-H/2, H/2]$ with W, H the width and height of the image.

The Nelder and Mead simplex algorithm [26], implemented as described in [27], is used to solve (1). This derivative-free optimization method evaluates iteratively $E(\Delta\phi)$ until a minimum is found. By simply changing the definition of $E(\Delta\phi)$, our approach can be readily adapted to a large class of similar problems. For instance, we have modified our method to use the SSIM

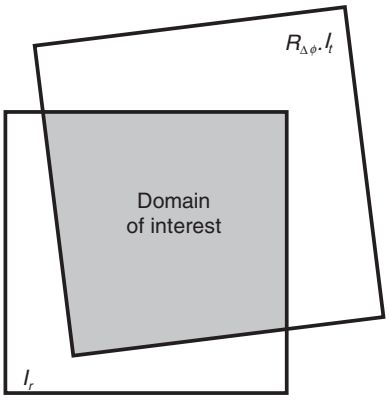

Figure 2

Domain of interest: intersection of two images.

(Structural SIMilarity) index [28] for finding the best parameters. We however found that the resulting algorithm is unstable for some pairs of images; for that reason, we advocate to use the MSE criterion given in Equation (2). Nevertheless, as shown by Figure 6, in section 1.5.3, minimizing the MSE turns out to also yield a better SSIM than conventional registration methods.

The initialization step deserves some explanations. The shifts $\Delta u_x, \Delta u_y$ are pre-estimated by means of cross-correlation. The rotation and scale parameters between two successive TEM images are very small: $\Delta\varphi$ does not exceed $\pm 2^\circ$ and Δs is in the range $\pm 0.5\%$; therefore, we start the optimization with $\Delta\varphi^{[0]} = 0$, $\Delta s^{[0]} = 0$ (neither rotation nor scaling change).

Note that, since $R_{\Delta\phi}$ is an interpolation operator which continuously depends on the parameters $\Delta\phi$, minimizing $E(\Delta\phi)$ achieves sub-pixel accuracy for the shift parameters.

1.2 Image Transformation

The linear operator $R_{\Delta\phi}$ in Equation (2) corresponds to the change of coordinates given by the matrix:

$$M_{\Delta\phi} = \begin{bmatrix} (s+\Delta s)\cos\Delta\varphi & (s+\Delta s)\sin\Delta\varphi & \Delta u_x \\ -(s+\Delta s)\sin\Delta\varphi & (s+\Delta s)\cos\Delta\varphi & \Delta u_y \\ 0 & 0 & 1 \end{bmatrix} \tag{3}$$

which depends on $\Delta\phi = (\Delta u_x, \Delta u_y, \Delta\varphi, \Delta s)$. The relation $v = M_{\Delta\phi} \cdot u$ changes the coordinates $u = (u_x, u_y, 1)^{\mathrm{T}}$ in the initial image into the coordinates $v = (v_x, v_y, 1)^{\mathrm{T}}$ in the transformed image. The transform $R_{\Delta\phi}$ is an interpolation operator. On the basis of many experiments, we have found that cubic B-spline interpolation [29] gives better results than nearest neighbors or linear interpolation methods.

1.3 Alignment of a Series of Projections

We now turn to the case of a series of projections. The first image is chosen as the reference image. By applying our alignment method for two images, each image is aligned with the previous image in the series, thereby sequentially compensating image shifts throughout the entire series. This method minimizes the following cost function:

$$E(\phi) = \sum_{t=1}^{M-1} \left(\frac{1}{N_t} \sum_{i=1}^{N_t} \left[I_t(u_i) - (R_{\Delta\phi_t} \cdot I_{t+1})(u_i) \right]^2 \right) \tag{4}$$

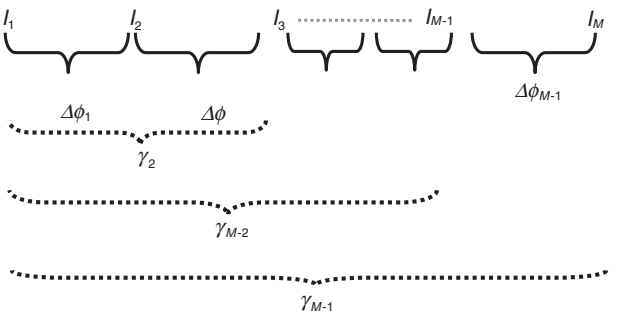

Figure 3

Correspondence between the transformation parameters of the image series.

where M is the number of images in the sequence, N_t is the number of pixels in the domain of interest between I_t and I_{t+1}, ϕ is a set of transformation parameters's vectors:

$$\phi = \{\Delta\phi_t\}_{t=1}^{M-1} \tag{5}$$

The form of function (4) allows parameters $\Delta\phi_t = (\Delta u_{t,x}, \Delta u_{t,y}, \Delta\varphi_t, \Delta s_t)$ associated with each pair of images to be determined in parallel. Figure 3 shows the relation between the transformation parameters in a series of images. $\gamma_t = (u_{t,x}, u_{t,y}, \varphi_t, s_t)$, $t = 1, \ldots, M-1$ are the pseudo-transformation parameters between images $2, \ldots, M$ and the first (reference) image. The components of γ_t are:

$$\begin{cases} u_{t,x} &= \text{Coeff.}(1,3) \text{ of } A_t \\ u_{t,y} &= \text{Coeff.}(2,3) \text{ of } A_t \\ \varphi_t &= \sum_{i=1}^{t} \Delta\varphi_i \\ s_t &= \prod_{i=1}^{t} \Delta s_i \end{cases} \tag{6}$$

with $A_t = R_{\Delta\phi_t} \cdot R_{\Delta\phi_{t-1}} \cdots R_{\Delta\phi_1}$.

1.4 Evaluation of the Alignment Accuracy

The SSIM index [28] measures the similarity between two images; we use it in order to check the efficiency of our method. The SSIM score, between -1 and 1, achieves its maximum value SSIM = 1 if and only if both images are identical. In our application, the SSIM index gives a degree of similarity in the domain of interest between the reference image and the registered image.

1.5 Experimental Results

For the following results, we use a series of TEM projections of a standard zeolite powder (CBV712 from *Zeolyst*). Our algorithm has been implemented and tested with Yorick (http://yorick.sourceforge.net/) on 2.6-GHz Intel Core 2 Duo machine. The computation time required for registration an image pair varies depending on the image size and the richness of texture content in the images.

1.5.1 Case Without Noise

In a first test, a 256×256 reference image I_r of 8-bit grayscale (*Fig. 4a*) is transformed into a new image I_t by applying a transformation $R_{\Delta\phi}$ to I_r with $\Delta\phi = (-5, 5, -10^\circ, -3\%)$. The corresponding SSIM (I_r, I_t) is 0.85. I_a is the image after registration of I_t on I_r using the proposed method. The residual image between I_a and I_r is shown in Figure 4b, with SSIM $(\mathrm{I_r}, \mathrm{I_a}) = 0.99$.

We return to the case of TEM images: $\Delta\varphi$ and Δs are very small. We generate a series of 140 random transformations, each consisting of a variation: Δu_x, $\Delta u_y \in [-30, 30]$, $\Delta\varphi \in [-0.5, 0.5]$, $\Delta s \in [-0.01, 0.01]$. We apply this transformation to I_r to create a series of test images. We then attempt to register each test image to I_r. The accuracy of the estimated translations $(\Delta u^*_{t,x}, \Delta u^*_{t,y})$ is given by computing the mean shift error:

$$\Delta_{shift} = \tfrac{1}{M}\sum_{t=1}^{M}\sqrt{(\Delta u_{t,x} - \Delta u^*_{t,x})^2 + (\Delta u_{t,y} - \Delta u^*_{t,y})^2},$$

for the estimated rotation $(\Delta\varphi^*_t)$ and scale (Δs^*_t):

$$\Delta_{\text{rotation}} = \tfrac{1}{M}\sum_{t=1}^{M}\sqrt{(\Delta\varphi_t - \Delta\varphi^*_t)^2},$$

$$\Delta_{\text{scale}} = \tfrac{1}{M}\sum_{t=1}^{M}\sqrt{(\Delta s_t - \Delta s^*_t)^2}.$$

M is the number of images. We show these values in Table 1.

1.5.2 Noisy Case

In this test, image I_t (*Fig. 5a*) is created by applying a transformation $R_{\Delta\phi}$ to I_r (*Fig. 4a*), with $\Delta\phi = (-5, 5, -10^\circ, -3\%)$ and adding Gaussian noise with zero mean and a standard deviation of $\sigma \leq 5.0$ pixels. The corresponding SSIM (I_r, I_t) is 0.83. Once I_r and I_t have been aligned, the residual image is very satisfactory (*Fig. 4b*, with SSIM $(I_r, I_a) = 0.97$).

We now add Gaussian noise ($\sigma \leq 5.0$ pixels) to each image of the series of test images, which is used in Section 1.5.1. The acquired images are then registered to I_r. We show the accuracy of the estimated translations, rotations and scales in Table 1.

1.5.3 Alignment of a Series of Projection

We have registered a series of TEM projections of size 256×256 of a zeolite catalyst support with our registration method (*Sect. 1.3*). The series contains 142 projections; the angle of tilt θ varies from -71° to $+70^\circ$ with a $+1^\circ$ increment. The projection which corresponds to $\theta = -71^\circ$, is presented in Figure 4a. We have compared the presented method to a robust standard method [18] which sequentially performs translation, rotation and scale registration. The cubic spline method [29] has been used for all interpolation procedures.

In Figure 6, higher score is better, the symbols (□) represent SSIM factors for the alignment of each pair of images using cross-correlation based approach, while the symbols (•) and the solid line (—) represent the

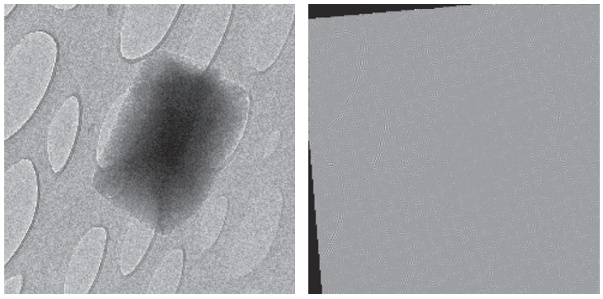

a) b)

Figure 4

a) Reference image of zeolite catalyst support I_r, b) difference between reference image I_r and aligned image I_a.

TABLE 1
The accuracy of the estimated translations, rotations and scales

	Δ_{shift} (pixel)	Δ_{rotation} (°)	Δ_{scale} (%)
No noise	0.187	6.7×10^{-3}	8.8×10^{-4}
Gaussian noise ($\sigma \leq 5.0$)	0.262	1.9×10^{-2}	3.4×10^{-3}

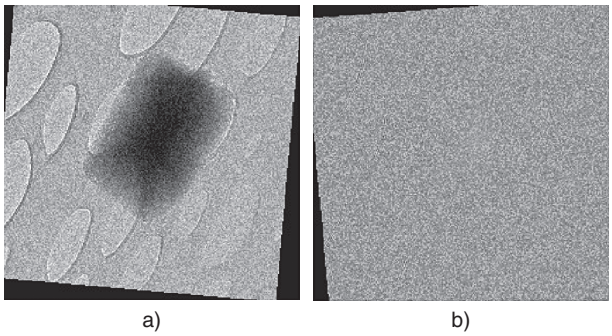

Figure 5

a) Image to be registered, b) residual image between I_r and I_a.

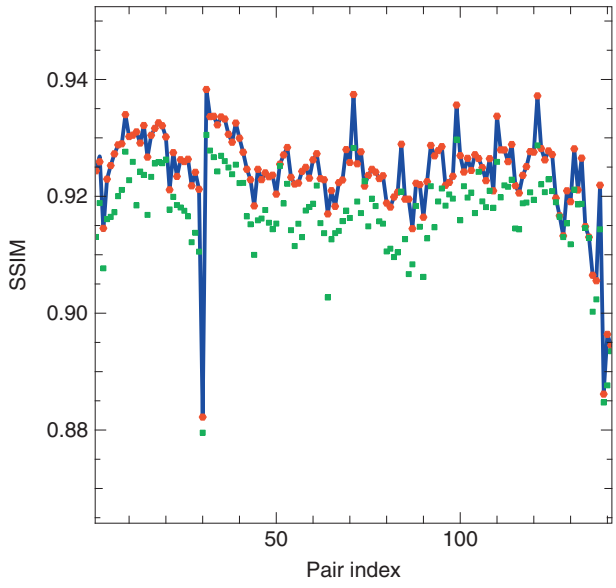

Figure 6

Values of the SSIM index for registrations obtained by standard robust sequential method (*green* □) [18] and by the proposed method based on: minimizing MSE (*red* •), or maximizing SSIM (*blue* –), evidencing a systematic higher scoring for our method.

SSIM factors for our method based on minimizing MSE or maximizing SSIM respectively. The presented registration method gives a higher similarity between the reference image and the registered image than the robust standard sequential approach.

We show in Figure 7 the MSE factors corresponding to the alignment of each pair of images by different methods, it shows clearly that the proposed methods have less errors with respect to the standard method.

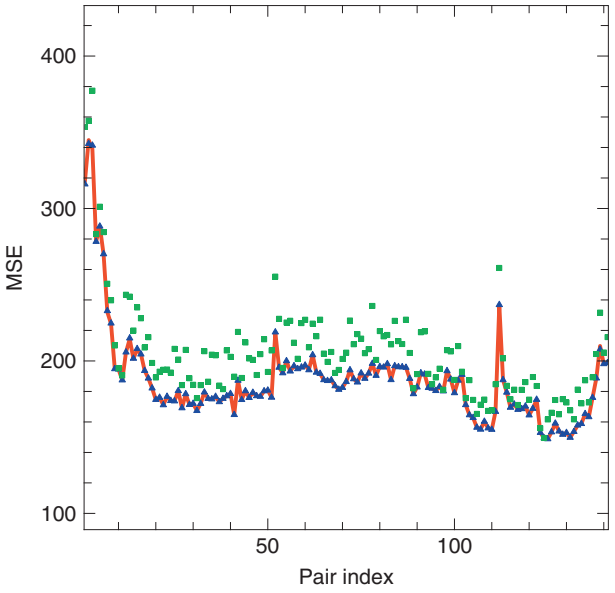

Figure 7

Values of the MSE index for registrations obtained by standard robust sequential method (*green* +) [18] and by the proposed method based on: maximizing SSIM (*blue* △), or minimizing MSE (*red* –), evidencing a systematic lower error for our method.

We conclude from Figures 6 and 7 that finding the best parameters by minimizing MSE or maximizing SSIM are essentially equivalent, while the accuracy obtained by a standard robust sequential method is lower.

For each pair of images, our method converges in 70 iterations on average, with total time ∼6.5 s, while the other method needs 4 s.

2 JOINT RECONSTRUCTION AND REFINED REGISTRATION

Typically, the tomography problem is represented by the relationship between the observed image (projections measurements) and the object to be reconstructed, which can be represented by the model:

$$I_t = H_{\phi_t} \cdot x + e_t \tag{7}$$

where $I_t \in \mathbb{R}^m$ corresponds to tomographic projections, which is observed on the detector (for the t^{th} projection), $x \in \mathbb{R}^n$ are the so-called voxels describing the object, $H_{\phi_t} \in \mathbb{R}^{m \times n}$ is a linear projection operator that characterizes how the projections are obtained from the object; the $\phi_t \in \mathbb{R}^6$ are orientation and position parameters of

the object with respect to the instrument (source + detector) for the acquisition of the t^{th} projection (see Appendix 1). In Equation (7), the term $e_t \in \mathbb{R}^m$ represents the errors due to the measurement noise and to the approximations of the model.

2.1 Solution of the Inverse Problem

The solution of the inverse problem is obtained by minimizing a cost function with respect to all voxels x and to all orientation parameters $\vartheta = \{\phi_t\}_{t=1}^{M}$, where M is the number of projections:

$$\{x, \vartheta\}^* = \arg\min_{x,\vartheta} f(x, \vartheta) \tag{8}$$

For statistically independent measures, the cost function is given by:

$$f(x, \vartheta) = \sum_{t=1}^{M} f_t(x, \phi_t) + f_{\text{prior}}(x) + \sum_{t=1}^{M} c_t(\phi_t) \tag{9}$$

with f_t the likelihood term of the t^{th} projection. For example, for a Gaussian noise:

$$f_t(x, \phi) = (I_t - H_\phi \cdot x)^{\mathrm{T}} \cdot W_t \cdot (I_t - H_\phi \cdot x) \tag{10}$$

where the weight matrix is the inverse of the covariance matrix of the noise: $W_t = \mathrm{Cov}(e_t)^{-1}$. The function $f_{\text{prior}}(x)$ strengthens the *priori* on the voxels x; the functions $c_t(\phi_t)$ introduce knowledge (measured or *a priori*) on the orientation parameters. A direct resolution of the problem as given by Equation (8) is impractical because it depends on many heterogeneous parameters (voxels, translations and angles). Moreover, the cost function is multimodal. In principle, a global optimization method is necessary. We therefore split this difficult problem into sub-problems easier to solve and for which we have effective methods of resolution.

2.2 Hierarchical Optimization

For given positional parameters ϑ, finding the best voxels amounts to a reconstruction formally given by:

$$x^+(\vartheta) = \arg\min_{x} f(x, \vartheta) \tag{11}$$

By plugging this solution into the cost function, we obtain a criterion depending only on ϑ:

$$f^+(\vartheta) = f(x^+(\vartheta), \vartheta) \tag{12}$$

The best positioning parameters are then obtained by solving an optimization problem of smaller size:

$$\vartheta^* = \arg\min_{\vartheta} f^+(\vartheta) \tag{13}$$

The solution of the global problem is then given by:

$$\{x, \vartheta\}^* = \{x^+(\vartheta^*), \vartheta^*\} \tag{14}$$

The reconstruction step, given by Equation (11), can be performed by an existing algorithm such as Filtered BackProjection (FBP) or by an algebraic reconstruction method from the pre-aligned projections (*Sect. 1.3*). However, the hierarchical optimization method is computationally too expensive to be applied directly. To accelerate the process, we use an alternating optimization approach (*Sect. 2.3*) which can however be sub-optimal compared to a hierarchical optimization.

2.3 Alternating Optimization

This method alternately estimates the voxels x for given positioning parameters ϑ and then estimates the parameters ϑ for given voxels x. This amounts to alternately perform volume reconstruction, Equation (11), and registration. As the voxels are considered fixed during the registration stage, each image can be registered independently (in parallel). In addition (see Appendix 1), the alignment of a projection can be done in a rather fast way by a re-interpolation of the projection model.

1. **Initialization**. Choose initial orientation parameters $\vartheta^{[0]}$ and let $k = 0$.
2. **Reconstruction**. Estimate the voxels given the positioning parameters $\vartheta^{[k]}$:
$$x^{[k+1]} = \arg\min_{x} f(x, \vartheta^{[k]}) \tag{15}$$
3. **Alignment**. For each projection, seek the best positioning parameters, with fixed voxels $x^{[k+1]}$:
$$\vartheta^{[k+1]} = \arg\min_{\vartheta} f(x^{[k+1]}, \vartheta)$$

For a separable cost function f like the one in Equation (9), the parameters ϕ_t associated with each projection are determined independently (that is, in parallel):

$$\phi_t^{[k+1]} = \arg\min_{\phi_t} f_t(x, \phi_t) + c_t(\phi_t) \tag{16}$$

Results are aggregated into:

$$\vartheta^{[k+1]} = \left\{\phi_t^{[k+1]}\right\}_{t=1}^{M}$$

4. **Convergence test**. If the method has converged (*e.g.*, the maximum magnitude of the translation alignment parameters is less than 1.0 pixels for two consecutive iterations), stop the iterations, otherwise increment k and return to step 2.

2.4 Results

In this section, we describe experimental results on the testing of our method using two data sets: a synthetic generated data and some series of TEM projections of standard zeolite powder. The computation time required for alternating optimization process depending separately on the time needed by the registration and the time spent for a reconstruction.

2.4.1 Algorithm Testing with Simulation Data

We suppose that we want to reconstruct one nanoparticle that has a single composition, embedded in a homogeneous support. Figure 8a shows a cross-section of the sample, orthogonal to the rotation axis of the tilt stage. The series contains 142 simulated projections (256×256 pixels^2) are computed from -71° to $+70^\circ$, using angular steps of $+1^\circ$. For simulation the misaligned images, due to the displacements of the sample, each image in the series is randomly transformed: horizontal and vertical shifts amount of at most $\pm 30\%$ of image dimensions, slightly rotations (does not exceed $\pm 0.5^\circ$) and small magnification changes (in the range $\pm 1.0\%$). To make the simulation more realistic, Gaussian noise with zero mean and a standard deviation of $\sigma \leq 5.0$ pixels is added to each of the projection images.

The coarse alignment process (*Sect. 1.5.3*) is applied on the simulation projection images. The aim is to reduce the strong shifts. From these pre-aligned projections, a first reconstructed volume is obtained by minimizing Equation (15) with a Quasi-Newton optimization algorithm: the limited memory Broyden-Fletcher-Goldfarb-Shanno (L-BFGS) method, combined with total-variation regularization [30]. We use a numerical model of projection (projector) based on cubic B-splines [31], which provides much less approximation errors than the distance driven projector [32].

Figure 8b shows a cross-section of the reconstructed volume corresponding to the cross-section shown in Figure 8a. The shape of the reconstructed particle is clearly distorted, due to the accumulation of errors in the coarse alignment process. This reconstructed volume is used to calculate the simulated views, which are then considered as reference images, that are matched with each initial projection. This process is repeated, the quality of the reconstruction has improved considerably in few iterations. Figure 8c shows the cross-section of the reconstruction using 2 iterations of refined registration process. It is already very clear that the quality of the reconstruction has improved considerably. Only 6 iterations are necessary to archive a good reconstruction (*Fig. 8d*), which is nearly perfect with respect to the original phantom. The quality improvement of the reconstructed volume at different iterations of alignment process is shown in Figure 9.

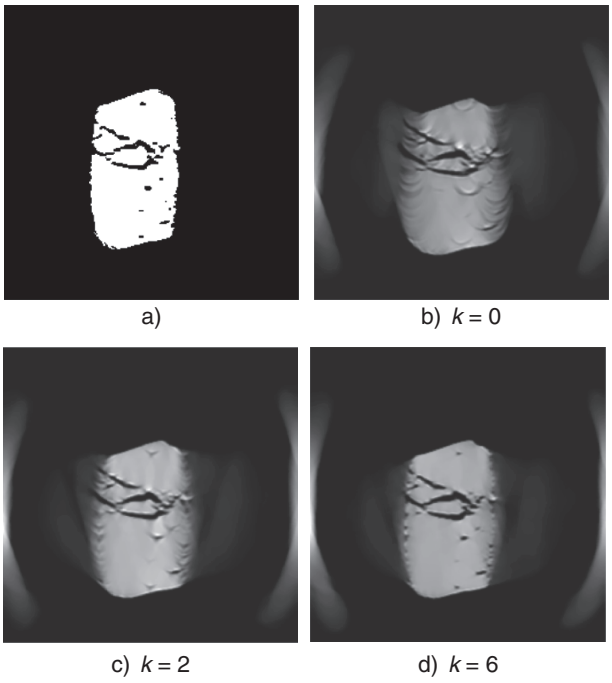

Figure 8

a) A cross-section of the original phantom, orthogonal to the rotation axis of the tilt stage. b-d) A cross-section of reconstructed volume using different numbers of iterations of refined registration process.

In the current implementation of the code, the time spent for a reconstruction by optimization using L-BFGS, is about 3 hours for a volume of $256 \times 256 \times 256$ voxels. This time can be reduced considerably by performing the reconstruction step by a standard reconstruction method as FBP, SIRT, ART, etc.; however, these methods can not perform regularized reconstruction, which is necessary to reduce artifacts due to missing projections (limited angle geometry).

2.4.2 Algorithm Testing with Experimental Data

In order to better understand the porosity of the zeolite powder (CBV712 from Zeolyst), we used electron

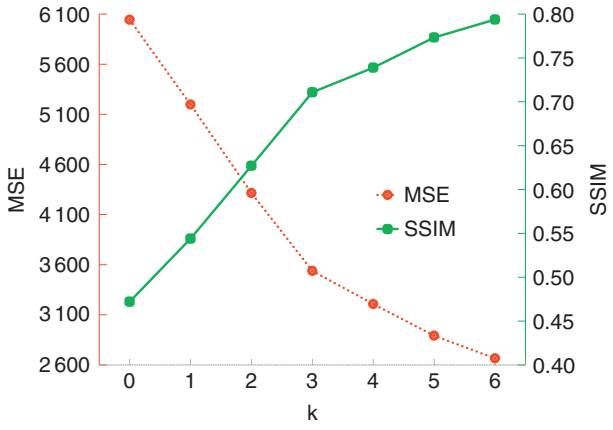

Figure 9

Values of the SSIM index and MSE between the original phantom and the reconstructed volume at different iterations.

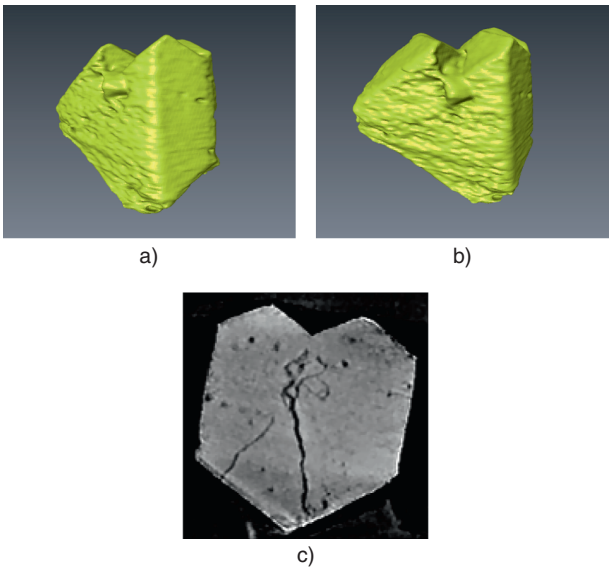

Figure 10

a,b) The isosurfaces of the final reconstruction obtained with the complete procedure with 256 × 256 TEM projections from different viewing angles. c) One slice in the *yz* direction of the reconstruction results.

tomography to evaluate the full 3D structure of the material. The tilt-series for the tomographic reconstruction was acquired on a TEM JEOL 2100F.

The first series of projections contains 142 images of a zeolite powder, which were acquired semi-automatically over a tilt range varying from $-71°$ to $+70°$. The projection which corresponds to $\theta = -71°$, is shown in Figure 4a. The series of images were aligned using our proposed approach.

We show in Figure 10a,b the isosurfaces of the final reconstruction, which is obtained after 6 iterations of the joint reconstruction and refined registration process. Figure 10c shows a cross-section in the *yz* direction of the final reconstruction which shows that even small details are reconstructed accurately.

Our second test used an other series of a zeolite powder, which contains 141 images from $-71°$ to $+69°$. The projections recorded at $\theta = -71°, 20°$ are shown in Figure 11a,b. We apply the same process of alignment. Figure 11c,d illustrate the isosurfaces of the final reconstruction obtained after 6 steps of iterations of registration process.

CONCLUSION

An automatic robust registration method using an inverse problem approach has been presented. Our experimental results demonstrate that the proposed method yields accurate translation, rotation and scaling parameters for electron tomographic series without needing fiducial markers.

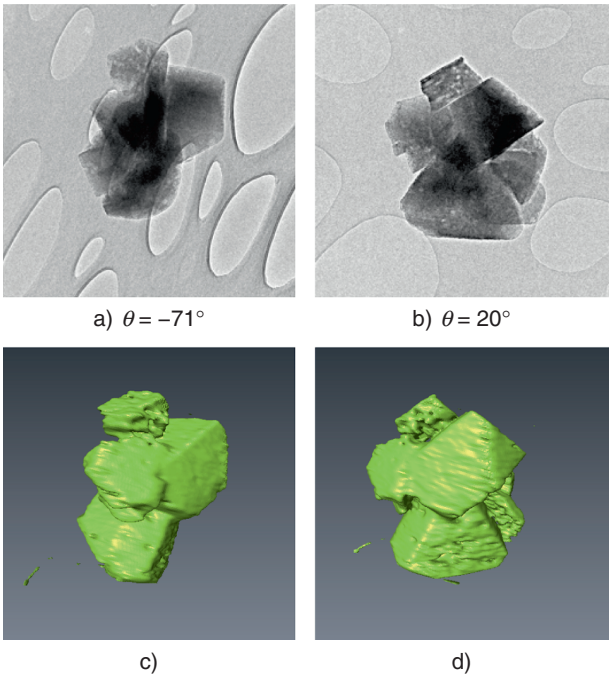

Figure 11

a,b) The real projections. c,d) The isosurfaces of the final reconstruction obtained after 6 steps of iterations of the joint reconstruction and refined registration process.

We are now working on a strategy to cope with missing projections by taking into account priors such as having a piecewise constant object with a very limited number of phases. This strategy will be integrated in the alternating optimization process to improve the quality of the reconstructed object in spite of instrumental jitter.

REFERENCES

1 Ersen O., Hirlimann C., Drillon M., Werckmann J., Tihay F., Pham-Huu C., Crucifix C., Schultz P. (2007) 3D-TEM characterization of nanometric objects, *Solid State Sci.* **9**, 12, 1088-1098.

2 Kak A.C., Slaney M. (1988) Principles of computerized tomographic imaging, *Engineering* **33**, 1, 327.

3 Gordon R., Bender R., Herman G.T. (1970) Algebraic Reconstruction Techniques (ART) for three-dimensional electron microscopy and X-ray photography, *J. Theor. Biol.* **29**, 3, 471-481.

4 Andersen A.H., Kak A.C. (1984) Simultaneous Algebraic Reconstruction Technique (SART): a superior implementation of the art algorithm, *Ultrason. Imag.* **6**, 1, 81-94.

5 Jiang M., Wang G. (2003) Convergence of the simultaneous algebraic reconstruction technique (SART), *IEEE Trans. Image Process.* **12**, 8, 957-61.

6 Crowther R.A. (1971) Procedures for three-dimensional reconstruction of spherical viruses by Fourier synthesis from electron micrographs, *Philos. Trans. R. Soc. Lon. B: Biol. Sci.* **261**, 837, 221-230.

7 Potts D., Steid G. (2000) New Fourier reconstruction algorithms for computerized tomography, *Wavelet Applications in Signal and Image Processing VIII Proc. SPIE* **4119**, 13-23.

8 Frank J. (2006) *Electron tomography: methods for three-dimensional visualization of structures in the cell*, Springer.

9 Ress D., Harlow M.L., Schwarz M., Marshall R.M., McMahan U.J. (1999) Automatic acquisition of fiducial markers and alignment of images in tilt series for electron tomography, *J. Electron Micros.* **48**, 3, 277-287.

10 Brandt S.S., Heikkonen J., Engelhardt P. (2001) Multiphase method for automatic alignment of transmission electron microscope images using markers, *J. Struct. Biol.* **133**, 3, 201-213.

11 Amat F., Moussavi F., Comolli L.R., Elidan G., Downing K.H., Horowitz M. (2008) Markov random field based automatic image alignment for electron tomography, *J. Struct. Biol.* **161**, 3, 260-275.

12 Brandt S.S., Heikkonen J., Engelhardt P. (2001) Automatic alignment of transmission electron microscope tilt series without fiducial markers, *J. Struct. Biol.* **136**, 3, 201-213.

13 Brandt S.S., Ziese U. (2006) Automatic TEM image alignment by trifocal geometry, *J. Microsc.* **222**, 1-14.

14 Sorzano C.O.S., Messaoudi C., Eibauer M., Bilbao-Castro J., Hegerl R., Nickell S., Marco S., Carazo J. (2009) Marker-free image registration of electron tomography tilt-series, *BMC Bioinformatics* **10**, 1, 124.

15 Frank J., McEwen B.F. (1992) Alignment by cross-correlation. *Electron Tomography Threedimensional Imaging with the Transmission Electron Microscope*, pp. 205-213, Plenum Press, New York.

16 Gratadour D., Mugnier L.M., Rouan D. (2005) Sub-pixel image registration with a maximum likelihood estimator application to the first adaptive optics observations of arp 220 in the L band, *Astron. Astrophys.* **365**, 357-365.

17 Liu Y., Penczek P.A., McEwen B.F., Frank J. (1995) A marker-free alignment method for electron tomography, *Ultramicroscopy* **58**, 3-4, 393-402.

18 Tzimiropoulos G., Argyriou V., Zafeiriou S., Stathaki T. (2010) Robust FFT-based scale-invariant image registration with image gradients, *IEEE Trans. Pattern Anal. Mach. Intell.* **32**, 10, 1899-1906.

19 Cop M., Dengler J. (1990) A multiresolution approach to the 3D reconstruction of a 50s ribosome from an EM-tilt series solving the alignment problem without gold particles, *Proceedings 10th International Conference on Pattern Recognition*, Atlantic City, NJ, 16-21 June.

20 Owen C.H., Landis W.J. (1996) Alignment of electron tomographic series by correlation without the use of gold particles, *Ultramicroscopy* **63**, 1, 27-38.

21 Winkler H., Taylor K.A. (2006) Accurate marker-free alignment with simultaneous geometry determination and reconstruction of tilt series in electron tomography, *Ultramicroscopy* **106**, 3, 240-254.

22 Houben L., Bar Sadan M. (2011) Refinement procedure for the image alignment in high-resolution electron tomography, *Ultramicroscopy* **111**, 9-10, 1512-20.

23 Penczek P.A., Grassucci R.A., Frank J. (1994) The ribosome at improved resolution: new techniques for merging and orientation refinement in 3D cryo-electron microscopy of biological particles, *Ultramicroscopy* **53**, 3, 251-270.

24 Yang C., Ng E.G., Penczek P.A. (2005) Unified 3-D structure and projection orientation refinement using quasi-newton algorithm, *J. Struct. Biol.* **149**, 1, 53-64.

25 Parkinson D.Y., Knoechel C., Yang C., Larabell C.A., Le Gros M.A. (2012) Automatic alignment and reconstruction of images for soft X-ray tomography, *J. Struct. Biol.* **177**, 2, 259-66.

26 Nelder J.A., Mead R. (1965) A simplex method for function minimization, *Comput. J.* **7**, 4, 308-313.

27 Lagarias J.C., Reeds J.A., Wright M.H., Wright P.E. (1998) Convergence properties of the Nelder-Mead simplex method in low dimensions, *SIAM J. Optim.* **9**, 1, 112.

28 Wang Z., Bovik A.C., Sheikh H.R., Simoncelli E.P. (2004) Image quality assessment: from error visibility to structural similarity, *IEEE Trans. Image Process.* **13**, 4, 600-612.

29 Thevenaz P., Blu T., Unser M. (2000) Interpolation revisited, *IEEE Trans. Med. Imag.* **19**, 7, 739-758.

30 Rudin L.I., Osher S., Fatemi E. (1992) Nonlinear total variation based noise removal algorithms, *Physica D* **60**, 259-268.

31 Momey F., Denis L., Mennessier C., Thiébaut E., Becker J.M., Desbat L. (2011) A new representation and projection model for tomography, based on separable B-splines, *IEEE Nuclear Science Symposium and Medical Imaging Conference (NSS/MIC) Record*, pp. 2602-2609.

32 DeMan B., Basu S. (2004) Distance driven projection and backprojection in three dimensions, *Phys. Medicine Biol.* **49**, 11, 2463-2475.

33 Soulez F., Denis L., Fournier C., Thiébaut E., Goepfert C. (2007) Inverse-problem approach for particle digital holography: accurate location based on local optimization, *J. Opt. Soc. Am. A* **24**, 4, 1164-1171.

Manuscript accepted in February 2013
Published online in October 2013

Copyright © 2013 IFP Energies nouvelles

Permission to make digital or hard copies of part or all of this work for personal or classroom use is granted without fee provided that copies are not made or distributed for profit or commercial advantage and that copies bear this notice and the full citation on the first page. Copyrights for components of this work owned by others than IFP Energies nouvelles must be honored. Abstracting with credit is permitted. To copy otherwise, to republish, to post on servers, or to redistribute to lists, requires prior specific permission and/or a fee: Request permission from Information Mission, IFP Energies nouvelles, fax. +33 1 47 52 70 96, or revueogst@ifpen.fr.

APPENDIX

1 Alignment of a Projection

For a given projection, there are 6 orientation parameters $\phi_t \in \mathbb{R}^6$: three translational ones: X_t, Y_t, Z_t and three rotational ones corresponding to three Euler angles $\beta_t, \psi_t, \alpha_t$. Since the considered system performs parallel projections, by an adequate choice of the axes (two axes OX, OY aligned with the pixels of the detector and the third one, OZ in the normal direction), 2 terms of translation X_t, Y_t correspond to a translation of the projection; the third one, Z_t, has an impact on the magnification of the projection; the angle of rotation α_t (around OZ) corresponds to a simple rotation of the projection in the detector plane (*Fig. A1*).

For 4 orientation parameters $(X_t, Y_t, Z_t, \alpha_t)$, the effects on projection can be obtained by simple interpolation. It remains two rotational angles β_t, ψ_t whose variation respectively around OY, OZ requires to recalculate the projection of the voxels. In mathematical terms:

$$H_{\phi_t+\Delta\phi_t} \cdot x \approx R_{\Delta\phi_t} \cdot H_{\phi_t} \cdot x$$

where R is a linear transformation similar to a 2D interpolation (translation, rotation and magnification) for a variation of parameters $\Delta\phi_t \in \mathbb{S}(\phi_t)$ belonging to some subspace $\mathbb{S}(\phi_t) \in \mathbb{R}^4$. This property should be exploited to accelerate the calculations. Otherwise, the effects of translation on the projection can be calculated for all possible translations with a pixel size resolution using a small number of FFT [33].

2 The Relationship Between the Presented Method and the Maximum Correlation

In order to keep things simple, we deal here with the case where two images I_1 and I_2 are misaligned only along a single dimension (OX). In such a case, the cost function is reduced to:

$$E(\Delta u, a) = \sum_{i=1}^{N} w_i \cdot [I_1(u_i) - a \cdot I_2(u_i - \Delta u)]^2$$

N is the number of pixels in the domain of interest (see *Fig. 2*), Δu the shift in position, a is a factor taking into account the attenuation, and w is a weighting function (which may be a function of u_i and $u_i - \Delta u$ the positions of the pixels that correspond in the two images). Minimizing $E(\Delta u, a)$ with respect to a:

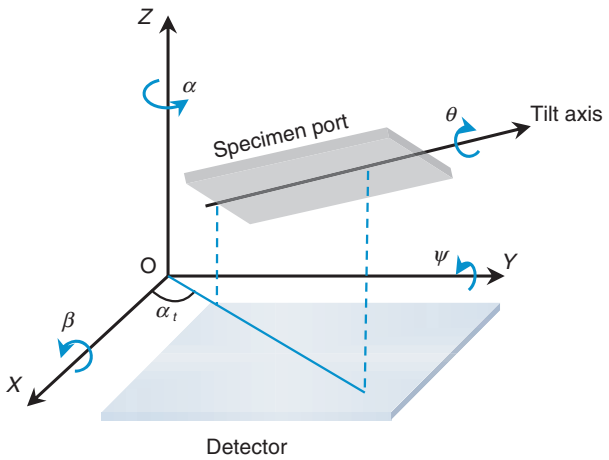

Figure A1

Tilt geometry: (X, Y, Z) coordinate system fixed. OZ is the optical axis. The OX, OY axes are parallel to the detector pixel rows and columns. The specimen port tilts about the tilt axis and angle θ. Due to mechanical imprecision, the specimen port may be shifted about X_t, Y_t, Z_t and slightly tilted about $\beta_t, \psi_t, \alpha_t$ (along/around OX, OY, OZ respectively).

$$\frac{\partial E(\Delta u, a)}{\partial a} = 0$$

we obtain:

$$a^{+}(\Delta u) = \frac{\sum_{i=1}^{N} w_i \cdot I_1(u_i) \cdot I_2(u_i - \Delta u)}{\sum_{i=1}^{N} w_i \cdot I_2(u_i - \Delta u)^2}$$

It is a function of Δu; by replacing in $E(\Delta u, a)$, we obtain a criterion which depends only on Δu:

$$E^{+}(\Delta u) = E(\Delta u, a^{+}(\Delta u)) = \sum_{i=1}^{N} w_i \cdot I_1(u_i)^2 - Q(\Delta u)$$

with:

$$Q(\Delta u) = \frac{\left[\sum_{i=1}^{N} w_i \cdot I_1(u_i) \cdot I_2(u_i - \Delta u)\right]^2}{\sum_{i=1}^{N} w_i \cdot I_2(u_i - \Delta u)^2}$$

As the first term of $E^{+}(\Delta u)$ does not depend on Δu, $E^{+}(\Delta u)$ is minimized with respect to Δu if and only if $Q(\Delta u)$ is maximized. Under the following assumptions:
1. the weights are constant (*i.e.* the noise level is the same for all pixels),
2. the denominator of $Q(\Delta u)$ is almost thesame whatever Δu,
3. and there is no contrast inversion between the two images (i.e. $a^{+}(\Delta u) > 0$),

the maximization of $Q(\Delta u)$ is equivalent to maximizing:

$$C(\Delta u) = \sum_{i=1}^{N} I_1(u_i) \cdot I_2(u_i - \Delta u)$$

(the numerator of $a^{+}(\Delta x)$ under the above assumptions) which is nothing else than the cross-correlation between the two images. While the 3rd assumption is reasonable, the two others are more obvious: the noise level may depend on the pixel and, if there are any structures in the images, the denominator of $Q(\Delta u)$ depend on Δu. Note that, if there are no such structures, registration is worthless so, at least, the 2nd assumption does not apply.

In fact, $E(\Delta u, a)$ can be seen as the opposite of the log-likelihood of the data given the model assuming Gaussian noise (not necessarily uniform). Thus, our approach derives from the maximum likelihood method by making less approximations (in particular the second one) than the maximum correlation method. For this reason, our method is likely to be superior.